Article

Enzyme-Free Liposome Active Motion via Asymmetrical Lipid Efflux

Jinyan Cui, Hui Jin, and Wei Zhan*

Read Online

ACCESS | Metrics & More | Article Recommendations | Supporting Information

ABSTRACT: As a class of biocompatible, water-dispersed colloids, liposomes have found widespread applications ranging from food to drug delivery. Adding mobility to these colloids, i.e., liposome micromotors, represents an attractive approach to next-generation liposome carriers with enhanced functionality and effectiveness. Currently, it remains unclear as to the scope of material features useful for building liposome micromotors or how they may differ functionally from their inorganic/polymer counterparts. In this work, we demonstrate liposome active motion taking advantage of mainly a pair of intrinsic material properties associated with these assemblies: lipid phase separation and extraction. We show that global phase separation of ternary lipid systems (such as DPPC/DOPC/cholesterol) within individual liposomes yields stable Janus particles with two distinctive liquid domains. While these anisotropic liposomes undergo pure Brownian diffusion in water, similar to their homogeneous analogues, adding extracting agents, cyclodextrins, to the system triggers asymmetrical cholesterol efflux about the liposomes, setting the latter into active motion. We present detailed analyses of liposome movement and cholesterol extraction kinetics to establish their correlation. We explore various experimental parameters as well as mechanistic details to account for such motion. Our results highlight the rich possibility to hierarchically design lipid-based artificial motors, from individual lipids, to their organization, surface chemistry, and interfacial mechanics.
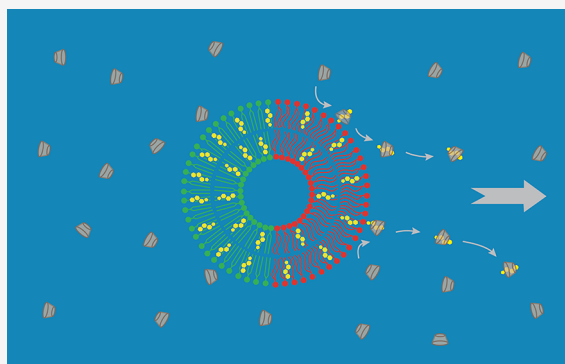
INTRODUCTION

Inspired by the elegance of natural microswimmers and enabled by recent advancement in material synthesis and microfabrication, research in microscopic artificial motors has blossomed into a field of extensive activity in recent years.[1−3] Such pursuit has been truly multidisciplinary, with chemists, engineers, and physicists often working side by side on the preparation, characterization, and theoretical formulation of these motors. Among the vast material and design choices being explored, spherical micromotors stand out for their simple geometry (with it, well-understood hydrodynamics) and ease of fabrication and thus have been essential to what the field has become today. Take Janus particles prepared from inorganic/polymer microbeads with partial metal coatings alone, for example, an array of mechanisms exploiting various catalytic,[4−6] photothermal,[7−9] and photocatalytic processes[10,11] offered by these materials have been demonstrated. In the majority of these cases, a local chemical/heat gradient across the particle/fluid interface drives the motion, whereas the particle's broken symmetry imparts direction.[12−14] With mobility as a built-in feature alongside their small size, these artificial motors promise exciting new application possibilities, including targeted drug delivery and microrobotics. To this end, however, the potential biotoxicity of these materials and their clearance from systems being treated often stand as significant issues to be reckoned with.[1−3,15]

As a closed spherical lipid assembly rich in surface/interfacial characteristics, liposomes represent an important class of water-dispersed colloids. Compared to their inorganic/polymer counterparts, from which the vast majority of existing nano- and micromotors are made, liposomes are ultimately economical in formation (i.e., all constituents surface bound and no hard/solid core) and biocompatible. These attractive features account for much of the industrial and medical use of liposomes,[16] e.g., in food,[17] drug delivery,[18] and cosmetics.[19] With added motility, particularly when furnished in a controlled and environmentally responsive manner, these liposome carriers will have much to gain in functionality and effectiveness.

Only a handful of studies have been reported using liposomes to achieve directional/active motion,[20] however. Taking a biohybrid approach, Kurakazu and co-workers attached flagella of *Chlamydomonas*, a biflagellate unicellular alga, to microsized liposomes, which display enhanced diffusion in the presence of ATP.[21] Similarly, Vanderlick et
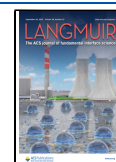
al. used *E. coli* to drive liposomes of different sizes.[22] Working with enzyme-coated liposomes with diameter on the order of 100 nm, researchers at Penn State have recently demonstrated enhanced (up to 25%) diffusion[23] as well as positive/negative chemotaxis[24] of liposomes in the presence of enzyme substrates. Decorating liposomes with catalytic Pt nanoparticles, Wang and co-workers demonstrated very recently a H_2O_2-responsive liposome nanomotor with high mobility and cell uptake rate,[25] in which clustering of nanoparticles on fluid lipid bilayers was utilized to achieve local reactivity and hence particle propulsion. As functional auxiliaries, liposomes have also been incorporated into artificial micromotor systems recently. For example, Städler et al. showed that the disintegration of liposomes coated on 0.8 μm silica beads could propel the latter along a gradient of lipid-dissolving agents.[26] All these studies, noticeably, are based on symmetrical liposomes with homogeneous surface makeup. On the use of Janus liposomes to achieve active/directional motion, only a couple of reports have appeared thus far. In the first, Inaba and co-workers demonstrated light-induced liposome propulsion using photocleavable peptides.[27] In our own work, we showed recently that dipolar (+/−) Janus liposomes undergo directional, domain orientation-specific motion driven by either an external electric field or interparticle electrostatic interactions.[28] These results point directly to the broken symmetry of Janus liposomes as an additional degree of freedom in manipulating liposome motion.

In this work, we investigate how interfacial lipid release from liposomes impacts their hydrodynamic behavior and demonstrate liposome active motion under asymmetrical lipid efflux conditions. Structurally, such asymmetry is realized via cholesterol-modulated liquid/liquid lipid phase separation[29−31] within individual liposomes, yielding Janus colloidal particles with two distinctive domains.[28,32] Adding β-cyclodextrin (β-CD), a cholesterol-extracting agent,[33,34] at low mM levels to the aqueous bulk then triggers cholesterol release from these Janus liposomes, which occurs at one domain an order of magnitude faster than the other. This asymmetrical material outflow, in turn, drives directional liposome movement against their Brownian diffusion. We further show how the active motion is correlated to liposome asymmetry and cholesterol extraction—the latter a surface-limited process sustained by continuous interdomain cholesterol transfer. We explore various experimental parameters as well as mechanistic details responsible for such motion. This work thus reveals a uniquely distinctive design principle based entirely on intrinsic physicochemical properties of lipid assemblies to achieve active motion.

RESULTS AND DISCUSSION

Liposome Motor Design and Tracking. The Janus configuration in individual liposomes is achieved through lipid phase separation in ternary lipid systems[29−31] consisting of a high-melting component (e.g., DPPC, melting temperature, T_m: 41 °C), a low-melting one (e.g., DOPC, T_m: −17 °C), and cholesterol (Chol), which yields a liquid-ordered (l_o) hemispherical bilayer domain and a liquid-disordered (l_d) half sharing a circular, quasi-1D phase boundary at room temperature (Figure 1). Such phase separation is thermodynamically favored, as it helps minimize free energy within the system caused by hard contact between DPPC and DOPC, whose acyl chains differ each other in physical dimension, order, and rotation/diffusion dynamics in bilayers.[35,36]
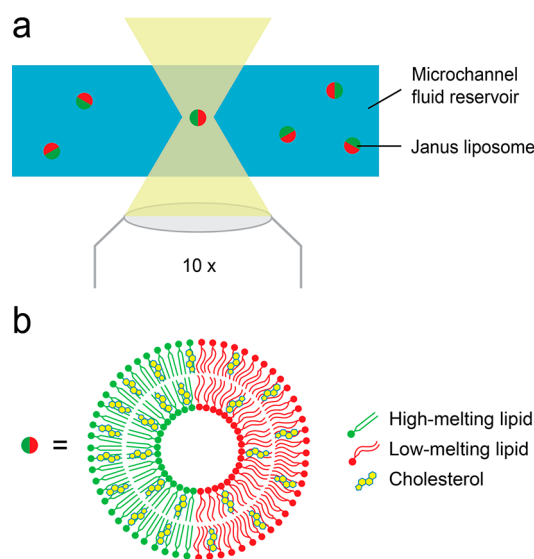

Figure 1. Liposome movement detection and liposome micromotor design. (a) Experimental setup for fluorescent monitoring of particle motion. (b) Schematic of liposome micromotor design, which features Janus liposomes composed of a high-melting lipid, a low-melting lipid, and cholesterol (Chol).

Compositionally, the l_o domain is enriched with DPPC/Chol and the l_d domain with DOPC.[37] By varying their mixing ratio at the stage of liposome formation, in addition, we can modify the relative size of the two domains in the end products.[32] To make these liposomes fluorescently accessible, we add low levels of rhodamine-labeled DOPE (rho-DOPE) and(/or) Bodipy-labeled cholesterol (Bodipy-Chol) in the lipid precursors. Of the two, rho-DOPE resides almost exclusively in the l_d domain,[38] whereas Bodipy-Chol is distributed in both domains with l_o-phase enrichment proportional to Chol.[39,40] Dilute suspensions (with volumetric fractions <0.01%) of thus labeled liposomes are loaded in transparent microchannel reservoirs, and their movement is then followed and recorded by a confocal fluorescence microscope (Figure 1a).

Upon addition of β-CD into the system, selective inclusion binding of Chol inside the former's cavity triggers a global Chol extraction from Janus liposomes. As detailed below, this interfacial material release takes place predominantly via the l_d domain, and, the resultant anisotropic traffic about the liposome causes the latter to move toward the extraction front against their Brownian diffusion. When either liposome asymmetry or Chol extraction is absent from the system, such directional motion ceases to occur. In the following sections, we present experimental evidence to confirm this new mode of active motion and analytically establish correlations between the extraction kinetics and active motion speed and finally discuss the mechanistic factors responsible for such motion.

Particle Trajectory Analysis Procedure and Benchmarking. To assess liposome movement quantitatively, we perform mean-square displacement (MSD) analysis on trajectories of individual liposomes. In 2D, this time-dependent quantity is expressed as $\text{MSD}(t) = \langle (x_{i+n} - x_i)^2 + (y_{i+n} - y_i)^2 \rangle$, where x_{i+n} and y_{i+n} denote coordinates of the particle's new location after time interval, n, whereas x_i and y_i represent its initial position. For spherical particles performing random walk only,[41,42] i.e., 2D diffusion, the ensemble-averaged MSD is related to their translational diffusion coefficient, D, by the linear relationship $\text{MSD}(t) = 4Dt$. In case that there exist
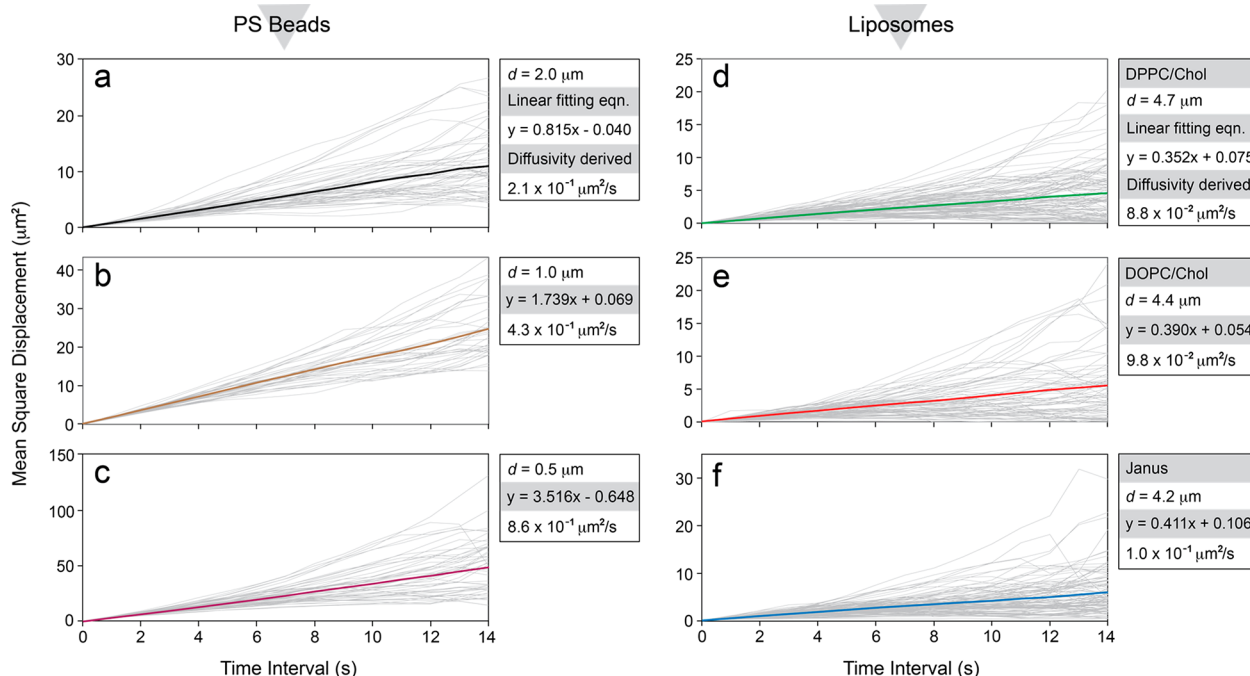
Figure 2. Mean-square displacement (MSD) plots of polystyrene (PS) microbeads (a–c) and liposomes (d–f) undergoing Brownian diffusion in DI water. In each case, the gray traces represent MSD plots averaged from all particles sampled in individual fluorescence videos, whereas the thick colored line is the ensemble-averaged MSD plot of all particles. The size, type of the particles, the linear fitting equation of their ensemble-averaged MSD, and calculated diffusion coefficient according to the Stokes–Einstein equation are presented in side panels. Lipid compositions: (d) DPPC/Chol (70/30, mol %), (e) DPPC/Chol (70/30), and (f) DPPC/DOPC/Chol (35/35/30); 0.1% Bodipy-Chol and/or rho-DOPE were also included in the liposome samples.

additional motional components in the system besides diffusion, the MSD plots obtained tend to deviate from linearity.[42,43] Because of the stochastic nature of thermal agitation, time-to-time and run-to-run fluctuations in MSD naturally occur even for particles of the same size. To uncover particle motion characteristics against such thermal randomness sufficiently accurately, it is thus necessary to sample sizable populations of liposomes so robust statistical analysis may be ensured. In our hands, we find such data convergence in microbead standards when more than 200 particles are sampled (Figure S1). A similar trend has been observed by others.[44] For our liposome samples, which are more polydisperse than the standards, we typically track and analyze 450–500 particles.

To test the effectiveness of our tracking procedure, we first studied the movement of fluorescent polystyrene (PS) microbeads (diameters: 0.5 ± 0.03, 1.0 ± 0.05, and 2.0 ± 0.2 μm) suspended in water. In each case, we obtained a linear ensemble-averaged MSD plot (Figure S2), indicative of pure Brownian diffusion. From the slope of these MSD plots, we then derived their diffusion coefficients (Figure 2a–c), which are in good agreement with values predicted independently by the Stokes–Einstein equation $D = kT/6\eta r$, where kT is the thermal energy term (4.07×10^{-14} cm^2 g s^{-2} at 22 °C), η the viscosity of the medium (9.54×10^{-3} g cm^{-1} s^{-1} for water at 22 °C), and r the radius of the particle: 2.26×10^{-9} cm^2 s^{-1} (2.0 μm), 4.53×10^{-9} cm^2 s^{-1} (1.0 μm), and 9.06×10^{-9} cm^2 s^{-1} (0.5 μm). These are uniformly greater than the MSD-derived values by 5–7%, which may be attributable to tracking inaccuracy, bead size distribution, and slight fluctuations in temperature.

All Liposomes Undergo Pure Brownian Motion in Water. With our tracking procedure giving satisfactory results for microbead standards, we next applied it to homogeneous (single-domain) and Janus liposomes. The size of these liposomes is controlled by extrusion using polycarbonate membranes with 5 μm diameter pores, yielding a population-weighted average diameter of 4.7 μm for DPPC/Chol, 4.4 μm for DOPC/Chol, and 4.2 μm for Janus liposomes (Figure S3). Here again, linear MSD plots are obtained for all three types of liposomes, suggesting that these lipid colloids undergo pure diffusion similar to their polymer counterparts, irrespective of lipid composition and phase conditions. From these linear plots, we once again derived their diffusivity values (Figure 2d–f), which are 5–9% lower than those obtained from Stokes–Einstein equation: 9.64×10^{-10} cm^2 s^{-1} (DPPC/Chol), 1.03×10^{-9} cm^2 s^{-1} (DOPC/Chol), and 1.08×10^{-9} cm^2 s^{-1} (Janus). Considering the significantly higher level of size dispersion in liposome samples (Figure S3), such a level of agreement is quite satisfactory.

Janus Liposomes Execute Active Motion under Cholesterol Extraction Conditions. To test the feasibility of exploiting lipid efflux for active liposome motion, we next examined liposome movement in the presence of β-CD. Owing to their high extraction efficiency and two-way binding dynamics, β-CD and its derivatives are widely employed in manipulating and controlling Chol level both in artificial and cellular lipid membranes.[45−47] Administered at relatively low (mM) levels, moreover, such extraction is Chol specific, with other coexisting lipid components such as phospholipids remain largely intact during the process.[48−50]

As shown in Figure 3a (traces in green and red), the MSD plots obtained from homogeneous DPPC/Chol and DOPC/
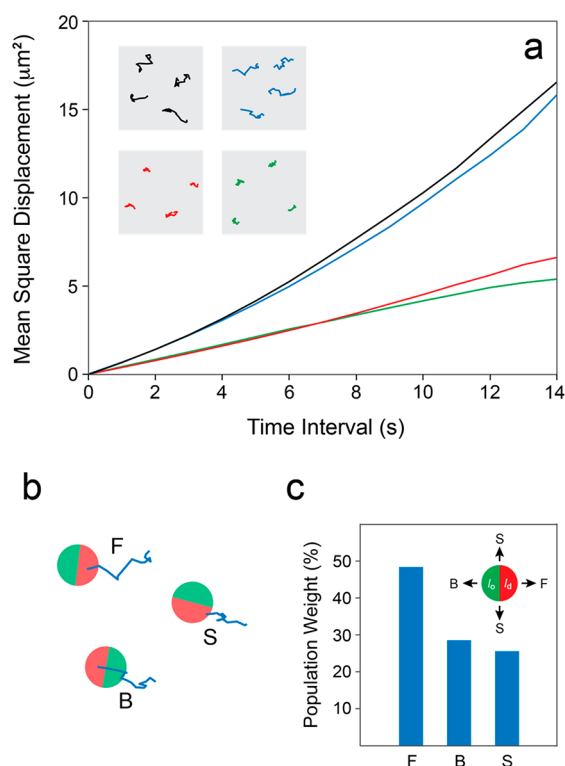
Figure 3. (a) MSD plots of homogeneous and Janus liposomes in the presence of 2 mM β-CD. Colors used for different samples: homogeneous DOPC/Chol (red), DPPC/Chol (green), DPPC/DOPC/Chol Janus (blue), and DPPC/DPhPC/Chol Janus (black). Insets: representative liposome movement trajectories; same color code applies. In each case, four individually collected trajectories are placed in a 25×25 μm^2 box (in gray). (b) Trajectory development vs Janus liposome initial orientation of the DPPC/DOPC/Chol sample: forward (F, with liposome's l_d domain as the front), backward (B), and sideways (S). (c) Population-wise ($n = 179$) analysis of liposome trajectory placement vs initial liposome orientation.

Chol liposomes remain largely linear in the presence of 2.0 mM β-CD. Their MSD-derived diffusion coefficients, 9.2 $\times$ 10^{-2} μm^2 s^{-1} (DPPC/Chol) and 9.3×10^{-2} μm^2 s^{-1} (DOPC/Chol), compare closely to those obtained in pure water. Strikingly, for Janus liposomes subjected to similar treatment, the resultant MSD plot displays greater stepwise displacements that yield an overall upward-bending profile (Figure 3a, blue trace), indicating the presence of active motion in the system besides diffusion.[42,43] A very similar trend is also observed when we extend the test to another Janus liposome system based on diphytanoylphosphatidylcholine (DPhPC) together with DPPC and Chol (Figure 3a, black trace). The motional difference between homogeneous and Janus liposomes is also evident from individual particle trajectories recorded (Figure 3a, inset). Because Chol extraction is expected to proceed similarly on homogeneous liposomes versus their corresponding domains on Janus liposomes (more below), the active motion observed most likely originates from the broken symmetry, i.e., the opposing l_d/l_o domains, associated with the latter.

Fitting these plots according to the two-component model,[12,42] $\mathrm{MSD}(t) = v_0^2 t^2 + 4Dt$, we further obtained the active motion velocity (v_0) and diffusivity (D) of the two Janus systems (Figure S4): 1.9×10^{-1} μm s^{-1} and 1.5×10^{-1} μm^2 s^{-1} (DPPC/DOPC/Chol); 2.0×10^{-1} μm s^{-1} and 1.6×10^{-1}

μm^2 s^{-1} (DPPC/DPhPC/Chol), respectively. Of the former, the calculated diffusivity is ~50% greater than that obtained in pure water, suggesting that diffusion is coupled with and enhanced by the active motion.[12,13] From these values, we also calculated Péclet number (Pe) associated with the active motion by Pe = $2rv_0/D$: 6.2 (DPPC/DOPC/Chol) and 6.5 (DPPC/DPhPC/Chol). A dimensionless quantity, Pe characterizes the relative contribution of active versus diffusive components to overall particle movement, with Pe $\gg$ 1 if active motion dominates in the system and Pe $\ll$ 1 when it is negligible. Thus, our Janus liposome system represents an intermediate case in which the active component is greater than but not dominant over diffusion. Of particular note is that due to time needed for solution mixing and injection (Experimental Section), our particle tracking procedure has to miss the initial stage of the extraction while the Chol efflux is the highest. Otherwise, we would expect to see more prominent liposome active motion.

A close examination of individual trajectories obtained from DPPC/DOPC/Chol Janus liposomes in addition reveals a direct correlation between the liposome trajectory placement and their initial domain orientation. Here, we define this correlation in three categories: front (with the trajectory developed in front of the l_d domain of the liposome), backward (with the trajectory developed in front of the l_o domain of the liposome), and sideways (Figure 3b). Expanding this analysis to the entire population ($n = 179$, with their initial domain orientation clearly identifiable), we find the forward case in 47% of the liposomes, whereas 28% went the opposite direction and 25% moved sideways (Figure 3c).

A related factor to consider here is liposome's rotational motion, which as thermal noise randomizes liposome orientation. For 5 μm diameter liposomes, we estimate their rotational diffusion coefficient (D_r) to be 1.03×10^{-2} s^{-1} by $D_r = kT/(8\eta r^3)$. From this value, we then obtain the persistence time associated with liposome motion (τ_r) at 48.5 s, following $\tau_r = [(d-1)D_r]^{-1}$, where d (=3) is the spatial dimension of rotation. Within the 15 s time window of liposome tracking, therefore, liposome active motion is expected to remain correlated to their initial orientation,[12,13] consistent with our experimental observation.

Cholesterol Extraction from Liposomes by β-CD Is Lipid Dependent and Domain Specific. To quantitatively assess Chol efflux in different lipid systems and thus identify its correlation with liposome motion, we next investigated Chol extraction kinetics by fluorescently following its analogue, Bodipy-Chol. Combining the dye's compact size and charge neutrality with Chol's main structural features in a small package, this probe has been found to closely track the distribution/transport of Chol in both model[45,46] and cellular[47,48] lipid environments. Moreover, Bodipy-Chol maintains similar emission characteristics in both l_d and l_o lipid domains,[51,52] enabling its use in following Chol partitioning among complex membrane phases. By combining fluorescence detection of Bodipy-Chol with external standard calibration (Experimental Section), we can thus quantify Chol levels in different liposomes and lipid domains.

As a preliminary test, our single-point fluorescence imaging reveals appreciably faster extraction on DOPC/Chol versus DPPC/Chol homogeneous liposomes. Upon 16 min continuous extraction, for example, Bodipy-Chol fluorescence is mostly retained in DPPC/Chol liposomes but largely lost from DOPC/Chol liposomes (Figure 4a). This trend is further

a

b
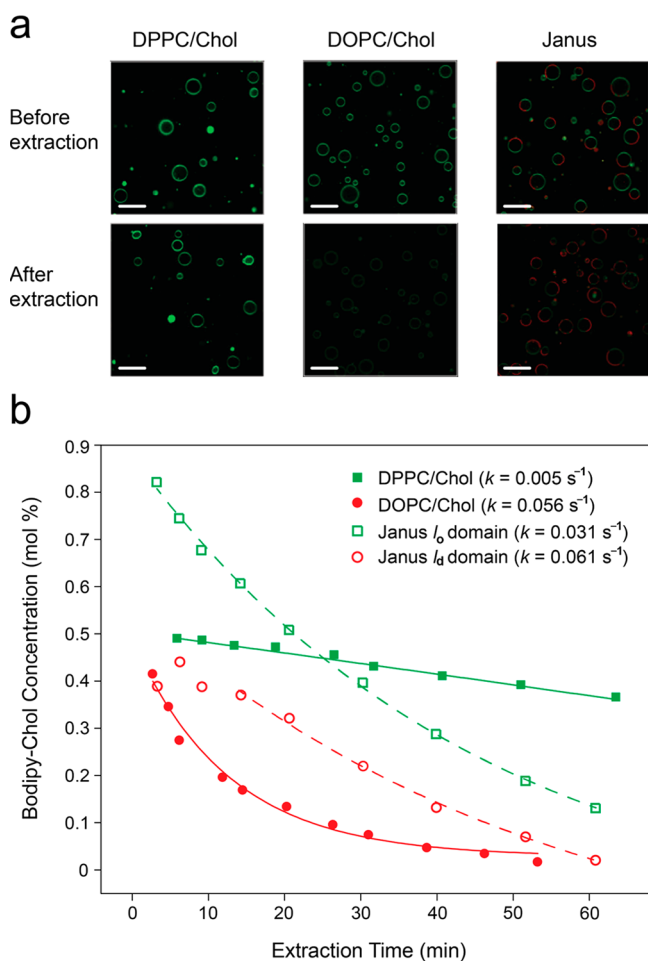
Figure 4. β-CD extraction of Chol from homogeneous and Janus liposomes. (a) Fluorescence micrographs of liposome samples before/after 16 min extraction with 2 mM β-CD. The concentration of Bodipy-Chol is 0.5% in homogeneous samples and 1% in Janus liposomes. Scale bar: 50 μm. (b) Bodipy-Chol concentration decrease in homogeneous (solid squares and circles) and Janus liposomes (open squares and circles) over time as a result of β-CD extraction. Solid and dashed lines are fitting curves obtained from first-order kinetics. In the case of the Janus l_d domain, only the last six data points were used to produce the fit.

confirmed by detailed time-dependent measurements, which identify first-order Chol extraction kinetics for both cases (Figure 4b). Specifically, it proceeds an order of magnitude faster in DOPC (k = 0.056 s^{-1}, $t_{1/2}$ = 9.5 min) compared to DPPC (k = 0.005 s^{-1}, $t_{1/2}$ = 143 min). This result is in accord with previous findings that Chol displays a higher tendency (activity) to escape from disordered lipid domains, a result due to complex interplay between Chol/lipid binding, lipid matrix order (with it, Chol's accessibility), and entropy.[53−55] Fast Chol extraction also appears evident at the l_d domain in Janus liposomes (Figure 4a).

Detailed kinetic analysis reveals several additional features unique to Janus liposomes (Figure 4b). To start, a rate constant of 0.031 s^{-1} ($t_{1/2}$ = 20 min) is found for Chol extraction at the l_o domain, which is 6 times higher than that from homogeneous DPPC liposomes. At the DOPC-enriched l_d domain, interestingly, the level of extraction appears to first rise at the beginning of the process before setting into a continuous decay (open circles in red, Figure 4b). The first-order fitting of the latter returns k = 0.061 s^{-1} ($t_{1/2}$ = 5.3 min),

which is quite comparable to that from homogeneous DOPC liposomes. Of the initial rise, it corresponds to a level of Chol traffic at the l_d domain that temporarily surpasses the local Chol availability. Because there exists no external Chol supply in the system, this greater Chol traffic can only be sustained by an *internal* Chol transfer, i.e., from the l_o to l_d domain, of the same Janus liposome. The existence of this internal route is also consistent with the observation of fast Chol depletion observed from the l_o domain, serving as the internal Chol reserve in the process. As suggested previously by Sanchez and co-workers,[56,57] the Chol distribution between l_o/l_d domains maintains a dynamic equilibrium dictated by the amount/type of lipids present in the liposome. When a preexisting equilibrium is tipped over by fast extraction taking place at one domain of the liposome, such internal Chol transfer acts to reestablish the global equilibrium.

Contributing Factors to Liposome Active Motion. Keeping the nominal liposome size constant at 5 μm, we next examined the impact of various extraction-related experimental variables on liposome motion. As for the concentration of the extracting agent, we find the MSD plot obtained with 0.5 mM β-CD to be closely comparable to the case of 2 mM β-CD (Figure 5a). When [β-CD] is raised to 4 mM, only a small (~10%) increase in liposome displacement is obtained (trace in purple, Figure 5a), which is likely due to the fast depletion of Chol from liposomes under high β-CD concentrations (see the Experimental Section). At still higher concentrations, e.g., 5 mM, substantial liposome morphological changes and rupturing prevent us from accurately identifying l_d/l_o domains. Interestingly, when we replace β-CD out from the system with methyl-β-CD (at 1 mM), a more efficient Chol-extracting agent than the former,[58,59] we observe a 35% enhancement in the resulting MSD (trace in orange, Figure 5a). Higher methyl-β-CD concentrations are not tested due to extensive liposome rupturing and lipid domain fusion.

Another factor investigated is the relative size of l_d versus l_o domains, i.e., the Janus ratio, in Janus liposomes, which can be controlled by adjusting the mixing ratio of the three main lipids.[32] Here, we identify a clear correlation, in that liposomes generally move more actively as their l_d domain becomes larger (Figure 5b). Of the three samples tested, the one prepared from DPPC/DOPC/Chol mixed at 50/20/30 (Janus ratio: ~1:3) produces the least active MSD plot, which is still significantly more active (by 90%) than that obtained from homogeneous DPPC/Chol liposomes under similar conditions (green trace at bottom, Figure 5b). In comparison, the 35/35/30 sample (Janus ratio: ~1:1) is 20% more active, which, in turn, is 47% slower than that from 30/50/20 mixed sample (Janus ratio: ~3:1). Of the latter, it is important to note that its highest mobility is achieved despite its lowest Chol level expected in the l_d domain among the three.[37] While these results point directly to the deciding role of liposome surface area on the liposome active motion, other factors, such as Chol anchoring strength and its heterogeneous liposome exit,[60] cannot be ruled out fully without further examination.

Molecular Interactions, Driving Forces and Hydrodynamics Involved. We now move on to a mechanistic discussion of the observed liposome active motion, focusing on the molecular interactions, interfacial forces, and hydrodynamics involved.
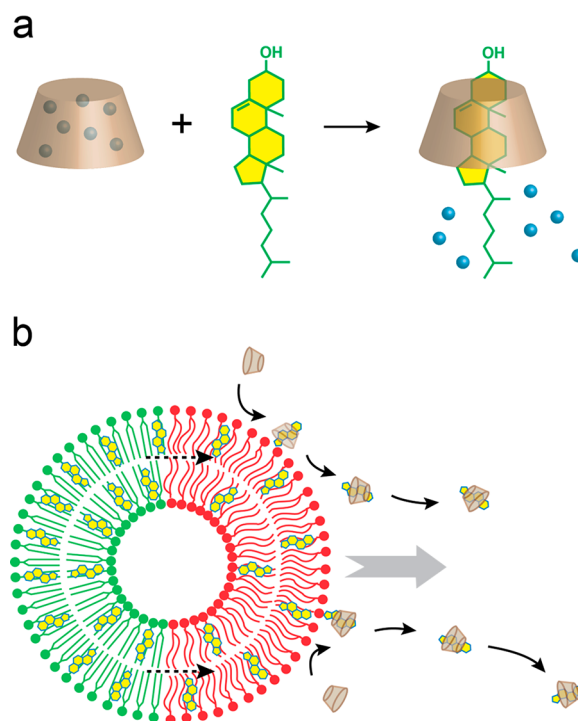
Starting from the extractant, β-CD, its α-1,4-linked, seven-member glucose ring system possesses a truncated-cone shaped structure when dispersed in water, featuring a shallow
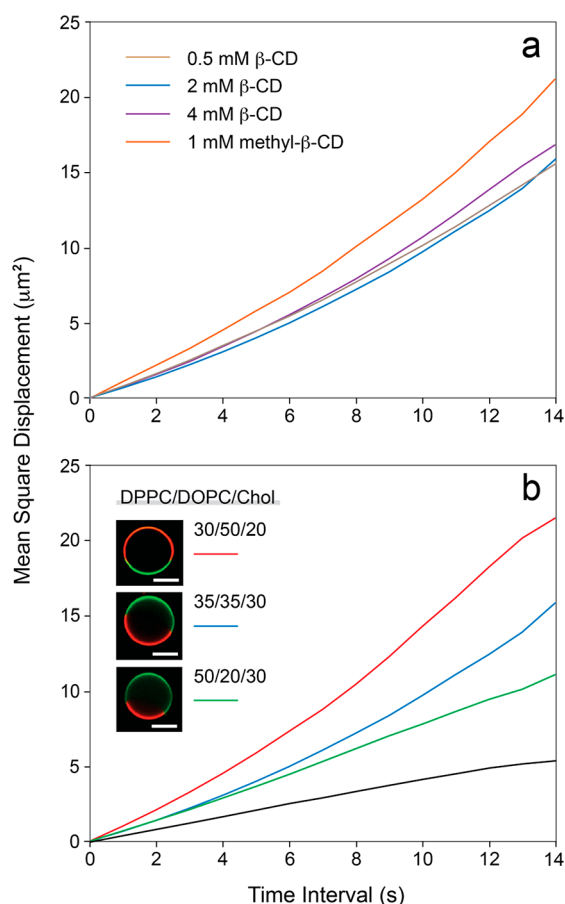
Figure 5. (a) MSD plots of Janus liposome movement obtained from different CD concentrations and types. (b) MSD plots of Janus liposome movement obtained from samples with different Janus ratios. The MSD plot obtained with DPPC/Chol liposomes under similar conditions is included as a reference (bottom trace in black). Inset: fluorescence micrographs of representative liposomes with different relative l_d/l_o domain sizes and their lipid mixing ratios. For clarify, these are taken from liposome samples without size control (extrusion). Scale bar: 10 μm.

Figure 6. (a) Schematic of CD/Chol inclusion complex formation and associated water release from CD's cavity. (b) Cartoon depiction of the driving force, lipid transfer (indicated by dashed arrows), and efflux (solid arrows) involved in the directional motion (gray arrow) of Janus liposomes.

hydrophobic cavity furnished distally by two (6-positioned) hydroxyl groups at the narrow end and four (2,3-positioned) hydroxyl groups at the other.[33] These peripheral hydroxyls render hydrogen bonding prominent in much of β-CD interaction with other species, be it a solvent (water primarily) or a binding partner. As to the cavity, it is important to recognize that it is "preloaded" with several water molecules inside, e.g., ~6 from neutron diffraction evidence.[61] Because of structural confinement presented by the cavity, moreover, these interior water molecules can only attain partial H-bonding, as opposed to the ideal 4-fold arrangement, with their neighbors. As such, they are highly disordered and mobile. When a binding partner enters β-CD's cavity to form an inclusion complex, out go these frustrated water molecules (Figure 6a). Energetically, it is the release of these high-energy waters to the bulk, thus restoring their H-bonding order, that primarily drives such formations.[62,63]

Once being added into a liposome solution, β-CD starts to accumulate around liposomes driven by H-bonding with the lipid headgroups.[64] From there, it would either thermally relax back to the bulk or, more eventfully, encounter a cholesterol nearby, whose hydroxyl group is positioned at the lipid/water

interface but less accessible to β-CD compared to coassembled phospholipids. Such encounters then trigger highly efficient Chol extraction from the liposome host, with ΔG estimated to be -40 kJ mol^{-1} for l_d-like lipid systems.[65] To pull the relatively long Chol fully out, the addition of second β-CD is favored so as to shield Chol's entire hydrophobic body from direct water exposure. This 2:1 CD⊃Chol complex stoichiometry is generally supported by experimental[66,67] and simulation[65,68] results. Once the extraction is complete, the resultant CD⊃Chol complex tends to diffuse away from the liposome surface—as a new entity, its concentration is the highest there. Such departure is also facilitated by the unbound β-CDs, which continuously diffuse in to replace those Chol-loaded ones from liposome surface and thus sustain the extraction. A two-way traffic of extractants, therefore, arises at the liposome/water interface (Figure 6b).

Mechanically, the extraction process can be viewed as an intermolecular tug of war between Chol's complexation with β-CD on one hand and Chol's anchoring in lipid matrices on the other. From recent single-molecule force studies, the former interaction registers a force of >30 pN,[69] exceeding the latter measured for both l_o (22 pN) and l_d (12 pN) bilayers[70] under comparable conditions. These results not only underscore β-CD's high extraction efficiency toward Chol, but, more importantly, they also hint at the pulling force that the liposome host must experience as Chol exits from it. As 2D liquids, l_o/l_d lipid bilayers are viscous matrices that exhibit internal friction. As the force imbalance causes Chol to accelerate from a relatively stationary starting position inside these matrices, part of momentum carried by Chol will be transferred to the liposome via such internal friction, resulting in a pull along the same direction, i.e., roughly perpendicular to

the local bilayer plane. Of the two CDs tested, methyl β-CD bears a deeper hydrophobic pocket that affords more favorable inclusion of Chol compared to β-CD,[71] thus registering a stronger pull. Its two H-bonds vs β-CD's six also translates to a smaller desorption energy barrier.[68] This pulling force, moreover, multiplies as the Chol efflux increases. Take homogeneous DOPC/Chol liposomes, for example. From the cross-section area each lipid occupies in a mixed lipid bilayer, 0.6 nm^2 for DOPC and 0.2 nm^2 for Chol,[72] we can estimate their average number in a 5 μm diameter unilamellar liposome: 2.2×10^8 and 1.0×10^8, respectively. Relating the latter with the extraction half-time obtained earlier ($t_{1/2}$ = 9.5 min), we can then obtain a rough estimate of the average Chol efflux: 1.1×10^3 μm^{-2} s^{-1}, which, notably, compares closely to the rate of β-CD-facilitated Chol desorption from mono-layers.[45]

Such Chol extraction-induced pulling does not produce directional liposome motion outright, however. Another key factor is the geometric asymmetry of Janus liposomes, which enables anisotropic Chol efflux over the liposome surface and, hence, external force development about the structure. By contrast, the spherical symmetry of homogeneous liposomes leads to net cancellation of interfacial forces around the particles. As a result, their motion remains largely diffusive despite their ongoing Chol extraction (Figure 3).

As the most abundant species present, water, particularly its hydration effect and associated hydrodynamics, needs specific consideration. For both homogeneous and Janus liposomes, we observe ideal Brownian motion (Figure 2) that can be fully described by diffusion of a rigid sphere at low Reynolds numbers.[41,73] Although there are no reported measurements on large liposomes as studied here, our result agrees with previous findings on diffusion of nanosized liposomes in dilute environments.[74,75] Microscopically, liposome diffusion results from uncompensated random thermal collisions by water molecules in the bulk. The bound waters, on the other hand, display much slower translational/rotational dynamics[76−78] and to a good approximation may be considered frozen during the collision process. In this sense, the bound water layer is as much on the receiving end of the collision as the liposome itself. As such, the bulk water "sees" and interacts with liposomes no differently than a hard sphere of the same size.

CONCLUSIONS

This work demonstrates liposome active motion through asymmetrical lipid efflux from Janus liposomes. Sustained by continuous Chol release from liposomes and interdomain Chol transfer, the observed active motion exceeds the background diffusion by nearly two-fold. By exploiting intrinsic material properties of lipid assemblies, such as lipid phase separation and extraction, this work represents a significant departure from existing liposome-based motor design strategies. Applied orthogonally together with the latter, it should enable further development of multiresponsive, function-programmable liposome motors. Largely a proof of concept in itself, this work outlines a hierarchical design principle that should be applicable to other lipid systems operating on alternative intermolecular interactions and interfacial properties. One of such possibilities for exploration is lipid active enzymes. Ongoing work in this laboratory is focused on improving the activity and robustness (e.g., under osmotic pressure or in crowded environments) of these liposome motors.

EXPERIMENTAL SECTION

Liposome Preparation. Janus as well as homogeneous liposomes were prepared by following the gel-assisted hydration method by Marques et al.[79] with minor modifications.[32] Briefly, dry poly(vinyl alcohol) (PVA, MW: 145000, Sigma-Aldrich) films were first prepared by spreading drops of a PVA aqueous solution (5 wt %) on precleaned glass slides, followed by drying at 50 °C for 0.5 h. On such dry PVA films, lipid stacks were then deposited by spreading small quantities of lipid precursors (e.g., 5 μL of 1 mM total lipids dissolved in chloroform) followed by further drying under vacuum for overnight at room temperature. In the final step, such dried lipid films were hydrated in DI water at 45 °C to yield liposomes. Depending on lipid composition, the hydration time varies: 1 h for homogeneous DPPC/Chol and DOPC/Chol liposomes; 2 h for DPPC/DOPC/Chol and DPPC/DPhPC/Chol Janus liposomes. The exact lipid compositions are specified in the main text. Unless specified otherwise, lipid-conjugated indicator dyes, 23-(dipyrrometheneboron difluoride)-24-norcholesterol (Bodipy-Chol, Avanti Polar Lipids) and/or 1,2-dioleoyl-sn-glycero-3-phosphoethanolamine-N-(lissamine rhodamine B sulfonyl) (ammonium salt) (rho-DOPE, Avanti Polar Lipids), were also included in the liposome formation at 0.1 mol %. Liposome samples thus prepared were stored at 4 °C for future use.

The size-controlled liposomes were prepared by extruding above-prepared hydration liposome samples one round through a plunger-based lipid extruder (Mini-Extruder, Avanti Polar Lipids) furnished by polycarbonate filter membranes with 5 μm diameter pores (Whatman Nuclepore, GE Healthcare). Fluorescence images of all liposomes before/after extrusion are included in Figure S3. The reported size of these liposomes was determined by the "Analyze Particles" function in ImageJ (ver.: 2.00-rc-69/1.52n).

Liposome Movement Tracking. Fluorescence images and videos of liposomes were acquired on a Nikon A1+/MP confocal scanning laser microscope (Nikon Instruments, Melville, NY) using 10× or 20× objectives and excitation laser lines at 488 and 561 nm. The corresponding green and red emission signals were filtered at 525 ± 25 and 595 ± 25 nm, respectively. For fluorescence recording, microscope-compatible, linear microfluidic channel slides (thinXXS 100182; dimensions: 200 μm × 200 μm × 18 mm; Cole-Parmer) were used as reservoirs to hold liposome samples. To avoid channel wall-associated motion complications and ensure run-to-run consistency, only particles near the center of microchannels, i.e., ~100 μm away from the channel sides and floor/ceiling, are monitored and recorded. Before each measurement, these microchannel slides were thoroughly cleaned by sonication for 30 min each in methanol and then DI water; residual solvents were blow-dried with a nitrogen stream. For PS bead and liposome diffusion measurements, dilute liposome samples in DI water were first pipetted into the microchannels. To achieve fluid quiescence, the liposome solution in the microchannel was sealed off from the surrounding at the two inlets with Parafilm. For liposome active motion measurement, dilute liposome samples in DI water were first mixed with cyclodextrin aqueous solutions of desired concentration, which were immediately injected into the microchannel, sealed, and secured on the stage of the fluorescence microscope. The whole procedure from sample mixing to the start of video recording is typically controlled under 2 min. Fluorescence videos were typically recorded at 512 × 512 pixel resolution at 1 frame/s, which represent the optimized conditions for us to be able to resolve Janus liposomes of 5 μm diameter and at the same time follow particle motion with sufficient time resolution. Several representative videos recorded for liposomes and PS microbeads are included in the Supporting Information. Unless otherwise specified, the final β-CD concentration is kept at 2 mM, which was chosen because (1) it elicits effective Chol extraction and (2) provides a long enough time window for reliable motion tracking and kinetics measurements. At 4 mM β-CD, by contrast, the extraction is found to ~85% complete in less than 5 min (data not shown).

Chol Extraction Kinetics. Home-prepared poly-(dimethylsiloxane) (PDMS, Sylgard 184, Dow Corning) microwells

(diameter: 5 mm; depth: 3 mm) fixed on glass slides were used as imaging cells for Chol extraction kinetics study. As samples, Bodipy-Chol labeled giant liposomes obtained directly from hydration (i.e., without size control by extrusion) were used. As detailed in the main text, we follow the extent of Chol extraction by imaging its fluorescent analogue, Bodipy-Chol, over the course of 60−70 min. To quantify its amount in liposome samples, calibration curves were first constructed from liposomes doped with known levels of Bodipy-Chol. For homogeneous samples, these are prepared at 0.1, 0.2, and 0.5 mol %, and for Janus liposomes, the series contains 0.2, 0.5, and 1 mol %, both yielding satisfactory linearity in the tested concentration range (Figure S5). To start each measurement, a 30 μL such liposome sample was first pipetted into a PDMS cell and given 0.5 h to settle; the liposome density is controlled such that this typically yields a dozen or so liposomes parked on the floor of the cell to start the measurement. To initiate the extraction process, a 30 μL 4 mM β-CD aqueous solution was gently pipetted into the liposome solution; the final β-CD concentration in the cell is thus 2 mM. To avoid fluorescence decay due to photobleaching, the samples are kept in dark unless during image acquisition. The fluorescence intensity of each sample was measured with the built-in intensity scan function in ImageJ, and the highest intensity corresponding to the liposome rim was reported (Figure S5).

Particle Trajectory Analysis. Monodisperse green fluorescent PS microbeads (diameters: 0.5 ± 0.03, 1.0 ± 0.05, and 2.0 ± 0.2 μm, Bangs Laboratories) were used to verify tracking accuracy of this procedure. Trajectories of both PS beads and liposomes are obtained by analyzing particle movement fluorescence videos using TrackMate, a single-particle tracking tool embedded in ImageJ. The trajectory files thus obtained were then imported into MATLAB to calculate the mean-squared displacement (MSD) of particle movement following a published protocol.[80] To ensure data convergence (Figure S1), at least 450 particles were analyzed in each sample to obtain the ensemble-averaged MSD plot.

ASSOCIATED CONTENT

Supporting Information

The Supporting Information is available free of charge at https://pubs.acs.org/doi/10.1021/acs.langmuir.2c01866.

> Additional experimental details, including mean-squared displacement (MSD) analysis data convergence, linear/quadradic fits of MSD plots of PS beads and liposomes, liposome size distribution upon extrusion and quantitative fluorescence analysis on individual liposomes (PDF)
> Video S1 (MP4)
> Video S2 (MP4)
> Video S3 (MP4)

AUTHOR INFORMATION

Corresponding Author

Wei Zhan − Department of Chemistry and Biochemistry, Auburn University, Auburn, Alabama 36849, United States; orcid.org/0000-0001-7096-9261; Email: wzz0001@auburn.edu

Authors

Jinyan Cui − Department of Chemistry and Biochemistry, Auburn University, Auburn, Alabama 36849, United States
Hui Jin − Department of Chemistry and Biochemistry, Auburn University, Auburn, Alabama 36849, United States

Complete contact information is available at:
https://pubs.acs.org/10.1021/acs.langmuir.2c01866

Notes

The authors declare no competing financial interest.

REFERENCES

(1) Sánchez, S.; Soler, L.; Katuri, J. Chemically Powered Micro- and Nanomotors. *Angew. Chem., Int. Ed.* **2015**, *54*, 1414−1444.

(2) Wong, F.; Dey, K. K.; Sen, A. Synthetic Micro/Nanomotors and Pumps: Fabrication and Applications. *Annu. Rev. Mater. Res.* **2016**, *46*, 407−432.

(3) Safdar, M.; Khan, S. U.; Jänis, J. Progress toward Catalytic Micro- and Nanomotors for Biomedical and Environmental Applications. *Adv. Mater.* **2018**, *30*, 1703660.

(4) Gibbs, J. G.; Fragnito, N. A.; Zhao, Y. Asymmetric Pt/Au Coated Catalytic Micromotors Fabricated by Dynamic Shadowing Growth. *Appl. Phys. Lett.* **2010**, *97*, 253107.

(5) Gao, W.; Pei, A.; Dong, R.; Wang, J. Catalytic Iridium-Based Janus Micromotors Powered by Ultralow Levels of Chemical Fuels. *J. Am. Chem. Soc.* **2014**, *136*, 2276−2279.

(6) Ma, X.; Jang, S.; Popescu, M. N.; Uspal, W. E.; Miguel-López, A.; Hahn, K.; Kim, D.-P.; Sánchez, S. Reversed Janus Micro/Nanomotors with Internal Chemical Engine. *ACS Nano* **2016**, *10*, 8751−8759.

(7) Wu, Y.; Si, T.; Lin, X.; He, Q. Near Infrared-Modulated Propulsion of Catalytic Janus Polymer Multilayer Capsule Motors. *Chem. Commun.* **2015**, *51*, 511−514.

(8) Jang, B.; Hong, A.; Kang, H. E.; Alcantara, C.; Charreyron, S.; Mushtaq, F.; Pellicer, E.; Büchel, R.; Sort, J.; Lee, S. S.; Nelson, B. J.; Pane, S. Multiwavelength Light-Responsive Au/B-TiO₂ Janus Micromotors. *ACS Nano* **2017**, *11*, 6146−6154.

(9) Liu, W.; Wang, W.; Dong, X.; Sun, Y. Near-Infrared Light-Powered Janus Nanomotor Significantly Facilitates Inhibition of Amyloid-B Fibrillogenesis. *ACS Appl. Mater. Interfaces* **2020**, *12*, 12618−12628.

(10) Xu, L.; Mou, F.; Gong, H.; Luo, M.; Guan, J. Light-Driven Micro/Nanomotors: From Fundamentals to Applications. *Chem. Soc. Rev.* **2017**, *46*, 6905−6926.

(11) Dong, R.; Cai, Y.; Yang, Y.; Gao, W.; Ren, B. Photocatalytic Micro/Nanomotors: From Construction to Applications. *Acc. Chem. Res.* **2018**, *51*, 1940−1947.

(12) Zöttl, A.; Stark, H. Emergent Behavior in Active Colloids. *J. Phys.: Condens. Matter* **2016**, *28*, 253001.

(13) Bechinger, C.; Di Leonardo, R.; Lowen, H.; Reichhardt, C.; Volpe, G.; Volpe, G. Active Particles in Complex and Crowded Environments. *Rev. Mod. Phys.* **2016**, *88*, 045006.

(14) Moran, J. L.; Posner, J. D. Phoretic Self-Propulsion. *Annu. Rev. Fluid Mech.* **2017**, *49*, 511−540.

(15) Xu, T.; Gao, W.; Xu, L.-P.; Zhang, X.; Wang, S. Fuel-Free Synthetic Micro-/Nanomachines. *Adv. Mater.* **2017**, *29*, 1603250.

(16) Lasic, D. D. Novel Applications of Liposomes. *Trends Biotechnol.* **1998**, *16*, 307−321.

(17) Gibbs, B. F.; Kermasha, S.; Alli, I.; Mulligan, C. N. Encapsulation in the Food Industry: A Review. *Int. J. Food Sci. Nutr.* **1999**, *50*, 213−224.

(18) Chang, H.-I.; Yeh, M.-K. Clinical Development of Liposome-Based Drugs: Formulation, Characterization, and Therapeutic Efficacy. *Int. J. Nanomedicine* **2012**, *7*, 49−60.

(19) Nohynek, G. J.; Lademann, J.; Ribaud, C.; Roberts, M. S. Grey goo on the Skin? Nanotechnology, Cosmetic and Sunscreen Safety. *Crit. Rev. Toxicol.* **2007**, *37*, 251−277.

(20) Santiago, I.; Simmel, F. C. Self-Propulsion Strategies for Artificial Cell-Like Compartments. *Nanomaterials* **2019**, *9*, 1680.

(21) Kurakazu, T.; Takinoue, M.; Kuribayashi-Shigetomi, K.; Takeuchi, S. Flagella-Driven Liposomes: Liposomes Actuated by Attached Flagella. *14th International Conference on Miniaturized Systems for Chemistry and Life Sciences*, Groningen, The Netherlands, 3−7 October 2010.

(22) Dogra, N.; Izadi, H.; Vanderlick, T. K. Micro-Motors: A Motile Bacteria Based System for Liposome Cargo Transport. *Sci. Rep.* **2016**, *6*, 29369.

(23) Ghosh, S.; Mohajerani, F.; Son, S.; Velegol, D.; Butler, P. J.; Sen, A. Motility of Enzyme-Powered Vesicles. *Nano Lett.* **2019**, *19*, 6019−6026.

(24) Somasundar, A.; Ghosh, S.; Mohajerani, F.; Massenburg, L. N.; Yang, T.; Cremer, P. S.; Velegol, D.; Sen, A. Positive and Negative Chemotaxis of Enzyme-Coated Liposome Motors. *Nat. Nanotechnol.* **2019**, *14*, 1129−1134.

(25) Wang, Z.; Yan, Y.; Li, C.; Yu, Y.; Cheng, S.; Chen, S.; Zhu, X.; Sun, L.; Tao, W.; Liu, J.; Wang, F. Fluidity-Guided Assembly of Au@Pt on Liposomes as a Catalase-Powered Nanomotor for Effective Cell Uptake in Cancer Cells and Plant Leaves. *ACS Nano* **2022**, *16*, 9019−9030.

(26) Mazur, F.; Fernández-Medina, M.; Gal, N.; Hovorka, O.; Chandrawati, R.; Städler, B. Locomotion of Micromotors Due to Liposome Disintegration. *Langmuir* **2020**, *36*, 7056−7065.

(27) Inaba, H.; Uemura, A.; Morishita, K.; Kohiki, T.; Shigenaga, A.; Otaka, A.; Matsuura, K. Light-Induced Propulsion of A Giant Liposome Driven By Peptide Nanofibre Growth. *Sci. Rep.* **2018**, *8*, 6243.

(28) Liu, Z.; Cui, J.; Zhan, W. Dipolar Janus Liposomes: Formation, Electrokinetic Motion and Self-Assembly. *Soft Matter* **2020**, *16*, 2177−2184.

(29) Veatch, S. L.; Keller, S. L. Separation of Liquid Phases in Giant Vesicles of Ternary Mixtures of Phospholipids and Cholesterol. *Biophys. J.* **2003**, *85*, 3074−3083.

(30) Veatch, S. L.; Polozov, I. V.; Gawrisch, K.; Keller, S. L. Liquid Domains in Vesicles Investigated by NMR and Fluorescence Microscopy. *Biophys. J.* **2004**, *86*, 2910−2922.

(31) Davis, J. H.; Clair, J. J.; Juhasz, J. Phase equilibria in DOPC/DPPC-d$_{62}$/cholesterol mixtures. *Biophys. J.* **2009**, *96*, 521−539.

(32) Wang, M.; Liu, Z.; Zhan, W. Janus Liposomes: Gel-Assisted Formation and Bioaffinity-Directed Clustering. *Langmuir* **2018**, *34*, 7509−7518.

(33) Szejtli, J. Introduction and General Overview of Cyclodextrin. *Chem. Rev.* **1998**, *98*, 1743−1753.

(34) Uekama, K.; Hirayama, F.; Irie, T. Cyclodextrin Drug Carrier Systems. *Chem. Rev.* **1998**, *98*, 2045−2076.

(35) Hofsäβ, C.; Lindahl, E.; Edholm, O. Molecular Dynamics Simulations of Phospholipid Bilayers with Cholesterol. *Biophys. J.* **2003**, *84*, 2192−2206.

(36) Orädd, G.; Westerman, P. W.; Lindblom, G. Lateral Diffusion Coefficients of Separate Lipid Species in a Ternary Raft-Forming Bilayer: A Pfg-NMR Multinuclear Study. *Biophys. J.* **2005**, *89*, 315−320.

(37) Veatch, S. L.; Soubias, O.; Keller, S. L.; Gawrisch, K. Critical Fluctuations in Domain-Forming Lipid Mixtures. *Proc. Natl. Acad. Sci. U. S. A.* **2007**, *104*, 17650−17655.

(38) Gudheti, M. V.; Mlodzianoski, M.; Hess, S. T. Imaging and Shape Analysis of GUVs as Model Plasma Membranes: Effect of Trans DOPC on Membrane Properties. *Biophys. J.* **2007**, *93*, 2011−2023.

(39) Ariola, F. S.; Li, Z.; Cornejo, C.; Bittman, R.; Heikal, A. A. Membrane Fluidity and Lipid Order in Ternary Giant Unilamellar Vesicles Using A New Bodipy-Cholesterol Derivative. *Biophys. J.* **2009**, *96*, 2696−2708.

(40) Wüstner, D.; Solanko, L.; Sokol, E.; Garvik, O.; Li, Z.; Bittman, R.; Korte, T.; Herrmann, A. Quantitative Assessment of Sterol Traffic in Living Cells by Dual Labeling with Dehydroergosterol and BODIPY-Cholesterol. *Chem. Phys. Lipids.* **2011**, *164*, 221−235.

(41) Berg, H. C. *Random Walks in Biology*; Princeton University Press: Princeton, NJ, 1983.

(42) Qian, H.; Sheetz, M. P.; Elson, E. L. Single Particle Tracking. Analysis of Diffusion and Flow in Two-Dimensional Systems. *Biophys. J.* **1991**, *60*, 910−921.

(43) Saxton, M. J.; Jacobson, K. Single Particle Tracking: Applications to Membrane Dynamics. *Annu. Rev. Biophys. Biomol. Struct.* **1997**, *26*, 373−399.

(44) Zhang, Y.; Hess, H. Chemically-Powered Swimming and Diffusion in the Microscopic World. *Nat. Chem.* **2021**, *5*, 500−510.

(45) Ohvo, H.; Slotte, J. P. Cyclodextrin-Mediated Removal of Sterols from Monolayers: Effects of Sterol Structure and Phospholipids on Desorption Rate. *Biochemistry* **1996**, *35*, 8018−8024.

(46) Leventis, R.; Silvius, J. R. Use of Cyclodextrins to Monitor Transbilayer Movement and Differential Lipid Affinities of Cholesterol. *Biophys. J.* **2001**, *81*, 2257−2267.

(47) Zidovetzki, R.; Levitan, I. Use of Cyclodextrins to Manipulate Plasma Membrane Cholesterol Content: Evidence, Misconceptions and Control Strategies. *Biochim. Biophys. Acta* **2007**, *1768*, 1311−1324.

(48) Kilsdonk, E. P. C.; Yancey, P. G.; Stoudt, G. W.; Bangerter, F. W.; Johnson, W. J.; Phillips, M. C.; Rothblat, G. H. Cellular Cholesterol Efflux Mediated by Cyclodextrins. *J. Biol. Chem.* **1995**, *270*, 17250−17256.

(49) Niu, S.-L.; Litman, B. J. Determination of Membrane Cholesterol Partition Coefficient Using A Lipid Vesicle−Cyclodextrin Binary System: Effect of Phospholipid Acyl Chain Unsaturation and Headgroup Composition. *Biophys. J.* **2002**, *83*, 3408−3415.

(50) Szente, L.; Fenyvesi, É. Cyclodextrin-Lipid Complexes: Cavity Size Matters. *Struc. Chem.* **2017**, *28*, 479−492.

(51) Sankaranarayanan, S.; Kellner-Weibel, G.; de la Llera-Moya, M.; Phillips, M. C.; Asztalos, B. F.; Bittman, R.; Rothblat, G. H. A Sensitive Assay for ABCA1-Mediated Cholesterol Efflux Using BODIPY-Cholesterol. *J. Lipid Res.* **2011**, *52*, 2332−2340.

(52) Sezgin, E.; Can, F. B.; Schneider, F.; Clausen, M. P.; Galiani, S.; Stanly, T. A.; Waithe, D.; Colaco, A.; Honigmann, A.; Wüstner, D.; Platt, F.; Eggeling, C. A Comparative Study on Fluorescent Cholesterol Analogs as Versatile Cellular Reporters. *J. Lipid Res.* **2016**, *57*, 299−309.

(53) McConnell, H. M.; Vrljic, M. Liquid-Liquid Immiscibility in Membranes. *Annu. Rev. Biophys. Biomol. Struct.* **2003**, *32*, 469−492.

(54) Ohvo-Rekilä, H.; Ramstedt, B.; Leppimäki, P.; Slotte, J. P. Cholesterol Interactions with Phospholipids in Membranes. *Prog. Lipid Res.* **2002**, *41*, 66−97.

(55) Lange, Y.; Steck, T. L. Cholesterol Homeostasis and the Escape Tendency (Activity) of Plasma Membrane Cholesterol. *Prog. Lipid Res.* **2008**, *47*, 319−332.

(56) Sanchez, S. A.; Tricerri, M. A.; Gratton, E. Interaction of High Density Lipoprotein Particles with Membranes Containing Cholesterol. *J. Lipid Res.* **2007**, *48*, 1689−1700.

(57) Sanchez, S. A.; Gunther, G.; Tricerri, M. A.; Gratton, E. Methyl-β-Cyclodextrins Preferentially Remove Cholesterol from the Liquid Disordered Phase in Giant Unilamellar Vesicles. *J. Membr. Biol.* **2011**, *241*, 1−10.

(58) Zidovetzki, R.; Levitan, I. Use of Cyclodextrins to Manipulate Plasma Membrane Cholesterol Content: Evidence, Misconceptions and Control Strategies. *Biochim. Biophys. Acta* **2007**, *1768*, 1311−1324.

(59) Kilsdonk, E. P. C.; Yancey, P. G.; Stoudt, G. W.; Bangerter, F. W.; Johnson, W. J.; Phillips, M. C.; Rothblat, G. H. Cellular Cholesterol Efflux Mediated by Cyclodextrins. *J. Biol. Chem.* **1995**, *270*, 17250−17256.

(60) Bacia, K.; Scherfeld, D.; Kahya, N.; Schwille, P. Fluorescence Correlation Spectroscopy Relates Rafts in Model and Native Membranes. *Biophys. J.* **2004**, *87*, 1034−1043.

(61) Betzel, C.; Saenger, W.; Hingerty, B. E.; Brown, G. M. Circular and Flip-Flop Hydrogen Bonding in β-Cyclodextrin Undecahydrate: A Neutron Diffraction Study. *J. Am. Chem. Soc.* **1984**, *106*, 7545−7557.

(62) Schneider, H.-J. Binding Mechanisms in Supramolecular Complexes. *Angew. Chem., Int. Ed.* **2009**, *48*, 3924−3977.

(63) Biedermann, F.; Nau, W. M.; Schneider, H.-J. The Hydrophobic Effect Revisited − Studies with Supramolecular Complexes

Imply High-Energy Water as A Noncovalent Driving Force. *Angew. Chem., Int. Ed.* **2014**, *53*, 11158−11171.

(64) Khuntawee, W.; Wolschann, P.; Rungrotmongkol, T.; Wong-Ekkabut, J.; Hannongbua, S. Molecular Dynamics Simulations of the Interaction of Beta Cyclodextrin with A Lipid Bilayer. *J. Chem. Inf. Model.* **2015**, *55*, 1894−1902.

(65) López, C. A.; de Vries, A. H.; Marrink, S. J. Computational Microscopy of Cyclodextrin Mediated Cholesterol Extraction from Lipid Model Membranes. *Sci. Rep.* **2013**, *3*, 2071.

(66) Tsamaloukas, A.; Szadkowska, H.; Slotte, P. J.; Heerklotz, H. Interactions of Cholesterol with Lipid Membranes and Cyclodextrin Characterized by Calorimetry. *Biophys. J.* **2005**, *89*, 1109−1119.

(67) Christoforides, E.; Papaioannou, A.; Bethanis, K. Crystal Structure of the Inclusion Complex of Cholesterol In *β*-Cyclodextrin and Molecular Dynamics Studies. *Beilstein J. Org. Chem.* **2018**, *14*, 838−848.

(68) López, C. A.; de Vries, A. H.; Marrink, S. J. Molecular Mechanism of Cyclodextrin Mediated Cholesterol Extraction. *PLoS Comput. Biol.* **2011**, *7*, e1002020.

(69) Pandey, S.; Xiang, Y.; Kankanamalage, D. V. D. W.; Jayawickramarajah, J.; Leng, Y.; Mao, H. Measurement of Single-Molecule Forces in Cholesterol and Cyclodextrin Host-Guest Complexes. *J. Phys. Chem. B* **2021**, *125*, 11112−11121.

(70) Stetter, F. W. S.; Cwiklik, L.; Jungwirth, P.; Hugel, T. Single Lipid Extraction: The Anchoring Strength of Cholesterol in Liquid-Ordered and Liquid-Disordered Phases. *Biophys. J.* **2014**, *107*, 1167−1175.

(71) Yu, Y.; Chipot, C.; Cai, W.; Shao, X. Molecular Dynamics Study of the Inclusion of Cholesterol into Cyclodextrins. *J. Phys. Chem. B* **2006**, *110*, 6372−6378.

(72) Pandit, S. A.; Chiu, S.-W.; Jakobsson, E.; Grama, A.; Scott, H. L. Cholesterol Packing Around Lipids with Saturated and Unsaturated Chains: A Simulation Study. *Langmuir* **2008**, *24*, 6858−6865.

(73) Batchelor, G. K. *An Introduction to Fluid Dynamics*; Cambridge University Press: New York, 1967.

(74) Haro-Pérez, C.; Quesada-Pérez, M.; Callejas-Fernández, J.; Casals, E.; Estelrich, J.; Hidalgo-Álvareza, R. Interplay between Hydrodynamic and Direct Interactions Using Liposomes. *J. Chem. Phys.* **2003**, *119*, 628−634.

(75) Yu, Y.; Anthony, S. M.; Bae, S. C.; Granick, S. How Liposomes Diffuse in Concentrated Liposome Suspensions. *J. Phys. Chem. B* **2011**, *115*, 2748−2753.

(76) König, S.; Sackmann, E.; Richter, D.; Zorn, R.; Carlile, C.; Bayerl, T. M. Molecular Dynamics of Water in Oriented DPPC Multilayers Studied by Quasielastic Neutron Scattering and Deuterium-Nuclear Magnetic Resonance Relaxation. *J. Chem. Phys.* **1994**, *100*, 3307−3316.

(77) Fitter, J.; Lechner, R. E.; Dencher, N. A. Interactions of Hydration Water and Biological Membranes Studied by Neutron Scattering. *J. Phys. Chem. B* **1999**, *103*, 8036−8050.

(78) Yang, J.; Calero, C.; Marti, J. Diffusion and Spectroscopy of Water and Lipids in Fully Hydrated Dimyristoylphosphatidylcholine Bilayer Membranes. *J. Chem. Phys.* **2014**, *140*, 104901.

(79) Weinberger, A.; Tsai, F.-C.; Koenderink, G.; Schmidt, T. F.; Itri, R.; Meier, W.; Schmatko, T.; Schöder, A.; Marques, C. Gel-Assisted Formation of Giant Unilamellar Vesicles. *Biophys. J.* **2013**, *105*, 154−164.

(80) Tinevez, J.-T.; Perry, N.; Schindelin, J.; Hoopes, G. M.; Reynolds, G. D.; Laplantine, E.; Bednarek, S. Y.; Shorte, S. L.; Eliceiri, K. W. TrackMate: An Open and Extensible Platform for Single-Particle Tracking. *Methods* **2017**, *115*, 80−90.